Available online at www.sciencedirect.com
ScienceDirect
Journal of Power Sources 159 (2006) 1346–1352
JOURNAL OF POWER SOURCES
www.elsevier.com/locate/jpowsour

Influence of nickel content on the chemical bonding character of $LiMn_{2-x}Ni_xO_4$ spinel oxides

Dae Hoon Park [a], Seung Tae Lim [a], Seong-Ju Hwang [a,*], Jin-Ho Choy [a,**], Jung Hyun Choi [b], Jaebum Choo [b]

[a] *Center for Intelligent Nano-Bio Materials (CINBM), Division of Nano Sciences and Department of Chemistry, Ewha Womans University, Seoul 120-750, Republic of Korea*
[b] *Department of Applied Chemistry and Chemistry, College of Science and Technology, Hanyang University, Ansan, Gyeonggi 425-791, Republic of Korea*

Received 25 October 2005; received in revised form 8 December 2005; accepted 8 December 2005
Available online 19 January 2006

Abstract

A relationship between the chemical bonding nature of $LiMn_{2-x}Ni_xO_4$ and the Ni content has been systematically investigated. According to X-ray diffraction analysis, nickel-substituted lithium manganates crystallize with a cubic spinel structure without the formation of any impurity phase such as NiO in the present substitution range of $0 \leq x \leq 0.4$. Micro-Raman analysis showed that Ni substitution gave rise to an increase in the intensities and energies of the two main phonon lines at ~580 and ~620 cm^{-1}, indicating enhancement of the average Mn oxidation states and reinforcement of the Mn—O bonds. This was confirmed by Mn K-edge X-ray absorption spectroscopic (XAS) analysis. Also, a new phonon line appeared at ~495 cm^{-1} after the Ni substitution, which can be assigned as an Ni–O vibration mode rather than as a $T_{2g}(2)$ mode of $LiMn_2O_4$. Ni K-edge XAS and micro-Raman analyses clearly demonstrate that divalent nickel ions existed in the octahedral sites of the cubic spinel lattice without a significant change in the chemical environment with the Ni content. In this regard, the poor electrochemical performance of heavily Ni-substituted compounds for the 3 V region is not attributable to the variation in the local environment of Ni ions with the Ni content, but to the low structural stability of the substituted NiO_6 octahedra.

Keywords: Chemical bonding nature; Cubic spinel lithium manganate; Nickel substitution; Micro-Raman spectroscopy; X-ray absorption spectroscopy

1. Introduction

The low toxicity, low price, and rich abundance of manganese have evoked intense research efforts to develop efficient manganese-based cathode materials for rechargeable lithium batteries [1]. Among various manganese oxides, spinel-structured lithium manganate has attracted special attention due to its high structural stability and facile synthesis. However, a remarkable capacity loss during the electrochemical charge–discharge process has inhibited the commercial use of this material. To circumvent this shortcoming, many attempts have been made to improve the electrochemical cyclability of the spinel compound [2–6]. Recently it was well established that the partial substitution of manganese ions with transition metal ions like Co, Cr, and Ni enhances the structural stability and electrochemical performance of the $LiMn_2O_4$ spinel [3,5]. There exists an optimum concentration of substituent ions for the best electrochemical performance of cation-substituted spinel compounds. For instance, a heavily Ni-substituted $LiMn_{2-x}Ni_xO_4$ ($x > 0.2$) phase has been known to show worse electrochemical performance, especially in the 3 V region, than a lightly Ni-substituted version with $x < 0.2$ [6]. Previously X-ray photoelectron spectroscopic (XPS) analysis on this system demonstrated that the oxidation state of the nickel ions varies depending on the Ni content, which was thought to be responsible for the negative effect in heavy Ni-substitution [7]. In addition, the partial occupation of Ni ions in the tetrahedral sites of the spinel lattice was suggested for the heavily Ni-

* Corresponding author. Tel.: +82 2 3277 4370; fax: +82 2 3277 3419.
** Corresponding author. Tel.: +82 2 3277 4135; fax: +82 2 3277 4340.
E-mail addresses: hwangsju@ewha.ac.kr (S.-J. Hwang), jhchoy@ewha.ac.kr (J.-H. Choy).

0378-7753/$ – see front matter © 2006 Elsevier B.V. All rights reserved.
doi:10.1016/j.jpowsour.2005.12.018

substituted compound. However, due to the surface sensitive nature of XPS, the chemical environment of the nickel ions in the bulk state has remained unclear [8]. In contrast to XPS, X-ray absorption spectroscopy (XAS) has been known to sensitively reflect the variation of local symmetry and electronic configuration of bulk species. Actually we have successfully utilized this method in the study of various electrode materials for lithium secondary batteries [9,10]. In combination with the XAS, micro-Raman spectroscopy is also useful in studying the crystal symmetry and bond strength of electrode materials [10–15].

In this study, we have investigated the crystal and electronic structures of the $LiMn_{2-x}Ni_xO_4$ spinel compounds by the combination of micro-Raman and XAS techniques. On the basis of the obtained information, we were able to determine the effect of the Ni content on the local chemical environment around the nickel substituent and to understand the variation of electrochemical performance of the spinel lithium manganate upon Ni substitution.

2. Experimental

The spinel $LiMn_{2-x}Ni_xO_4$ ($0 \le x \le 0.4$) samples were prepared by heating the stoichiometric mixture of Li_2CO_3, Mn_2O_3, and NiO at 730–750 °C for 40 h with intermittent grindings [3]. The crystal structures of these spinel-structured materials were studied by powder X-ray diffraction (XRD) using Ni-filtered Cu Kα radiation with a graphite diffracted beam monochromator. Micro-Raman spectra presented here were recorded on a Renishaw instrument coupled with an optical microscope (spatial resolution of 1 μm^2). The samples were excited with the 514.5 nm line of an Ar^+ laser. All the present spectra were obtained by backscattering from the powdered sample or from freshly cleaved surfaces of a polycrystalline sample. The resolution of the present spectra was 3–4 cm^{-1}. In order to prevent possible thermal damage to the sample, the power of the incident laser light was maintained at lower than 5 mW. After each measurement, the sample surface was thoroughly checked to remove the possibility of spectral modification caused by the surface degradation. XAS experiments were carried out at the Ni K- and Mn K-edges by using the extended X-ray absorption fine structure (EXAFS) facility installed at the beam line 7C at the Pohang Light Sources (PLS) in Korea, operated at 2.5 GeV and 180 mA. XAS data were collected at room temperature in a transmission mode using a Si(1 1 1) single crystal monochromator and gas-ionization detectors. All the present spectra were calibrated carefully by measuring the reference spectra of the Ni or Mn metal simultaneously. Data analysis for the experimental spectra was carried out using the standard procedure [16]. In the course of EXAFS fitting analysis, the coordination number (CN) was fixed to the crystallographic values while the amplitude reduction factor (S_0^2) was allowed to vary. The best-fit S_0^2's of all the present $LiMn_{2-x}Ni_xO_4$ and the reference NiO are consistent with one another within 10% deviation. All the bond distances (R), Debye-Waller factors (σ^2), and energy shifts (ΔE) were set as variables.

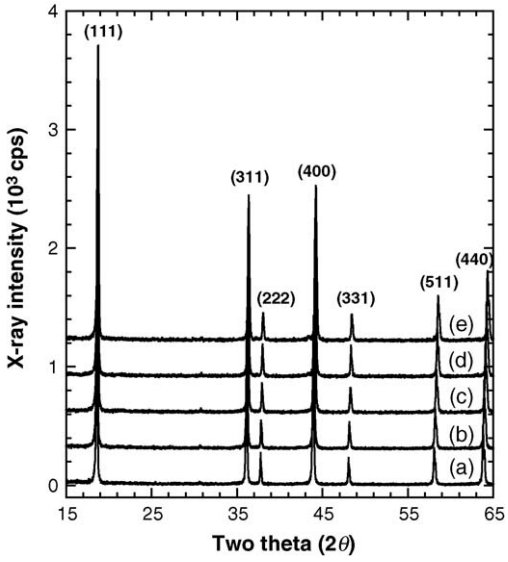

Fig. 1. Powder XRD patterns for the nickel-substituted $LiMn_{2-x}Ni_xO_4$ spinel compounds with x = (a) 0, (b) 0.1, (c) 0.2, (d) 0.3, and (e) 0.4.

3. Results and discussion

3.1. Powder XRD analysis

Fig. 1 represents the powder XRD patterns of nickel-substituted $LiMn_{2-x}Ni_xO_4$ ($0 \le x \le 0.4$) spinel oxides. All of the present compounds show nearly the same patterns with well-developed ($h\,k\,l$) reflections, which can be well indexed on the basis of the cubic spinel structure with the space group of Fd-3m [3]. No trace of an impurity phase like NiO is observable in the present patterns, indicating the formation of single-phase cubic spinel compounds in the present Ni substitution range. The lattice parameters and unit cell volumes of these spinel-structured compounds were calculated from least square fitting analysis, as summarized in Table 1. The replacement of Mn with Ni gives rise to the shrinkage of the unit cell volume, even though the substituent Ni^{II} ion possesses a larger radius than manganese ions ($Mn^{III}(6) = 0.65$ Å, $Mn^{IV}(6) = 0.53$ Å, and $Ni^{II}(6) = 0.70$ Å, where the number in parentheses represents the coordination number [17]). Such a lattice contraction upon Ni substitution suggests that the lattice parameter of the spinel lithium manganate is mainly dependent on the average oxidation state of manganese, which is enhanced by the Ni substitution.

Table 1
Lattice parameter a, unit cell volume (V_c), and crystal symmetry of nickel-substituted lithium manganese oxides

Compound	a (Å)	V_c	Crystal symmetry
$LiMn_2O_4$	8.251	561.72	Cubic
$LiMn_{1.9}Ni_{0.1}O_4$	8.236	558.66	Cubic
$LiMn_{1.8}Ni_{0.2}O_4$	8.218	555.01	Cubic
$LiMn_{1.7}Ni_{0.3}O_4$	8.203	551.97	Cubic
$LiMn_{1.6}Ni_{0.4}O_4$	8.187	548.75	Cubic

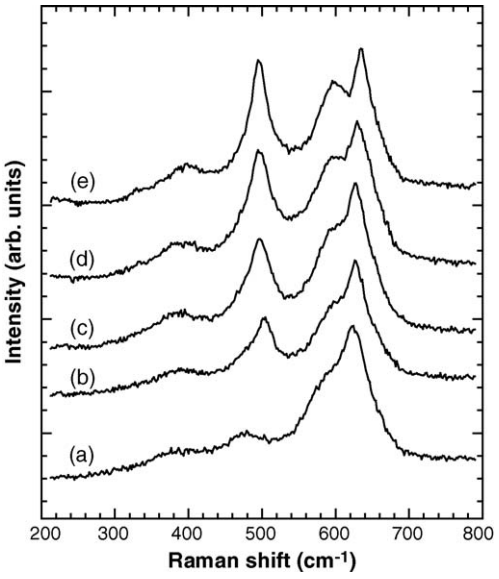

Fig. 2. Micro-Raman spectra for the nickel-substituted $LiMn_{2-x}Ni_xO_4$ spinel compounds with x = (a) 0, (b) 0.1, (c) 0.2, (d) 0.3, and (e) 0.4.

3.2. Micro-Raman analysis

The effects of Ni substitution on the lattice vibration and bond strength of cubic spinel lithium manganate have been examined using micro-Raman spectroscopy. The micro-Raman spectra of the cubic spinel $LiMn_{2-x}Ni_xO_4$ ($0 \le x \le 0.4$) are presented in Fig. 2, together with those of cubic spinel λ-MnO_2 and tetragonal spinel $Li_2Mn_2O_4$ compounds. Although factor group analysis predicts five Raman active modes ($A_{1g} + E_g + 3T_{2g}$) for the cubic spinel $LiMn_2O_4$ [12], only four Raman peaks are discernible in the present spectra of $LiMn_2O_4$. Except for the absence of several weak features, the overall spectral feature of unsubstituted $LiMn_2O_4$ compound appears to be very close to the previously reported ones [9,12,13]. On the basis of a theoretical energy calculation and a comparative study of Cr-substituted $LiMn_{2-x}Cr_xO_4$ [9,12], two intense Raman features at ~580 and ~620 cm^{-1} were assigned as A_{1g} modes for regular $Mn^{IV}O_6$ octahedra and tetragonally distorted $Mn^{III}O_6$ octahedra, respectively. Weak phonon lines at ~370 and ~470 cm^{-1} are attributable to the Raman active $T_{2g}(1)$ and $T_{2g}(2)$ modes, whereas the $T_{2g}(3)$ phonon line would be concealed by the intense A_{1g} peak [9]. Although a phonon line corresponding to the E_g mode was reported to appear at 432 cm^{-1} [12], it is absent in the present spectrum, which might be due to its very weak intensity and diffusive feature. The substitution of Mn with Ni gives rise to several significant variations in the Raman spectra; the first is the variation of the relative intensity between the two strong features at around 580 and 620 cm^{-1}, as plotted in Fig. 3a. As the Ni content increases, the peak at ~580 cm^{-1} becomes enhanced with respect to the peak at ~620 cm^{-1}. On the basis of the peak assignment, such an increase of the relative intensity of 580/620 cm^{-1} peaks can be regarded as strong evidence for the increase of average Mn oxidation state. In fact, similar spectral change was also observed for the Cr-substituted $LiMn_{2-x}Cr_xO_4$ system [9]. In addition to the variation of spectral weights, these

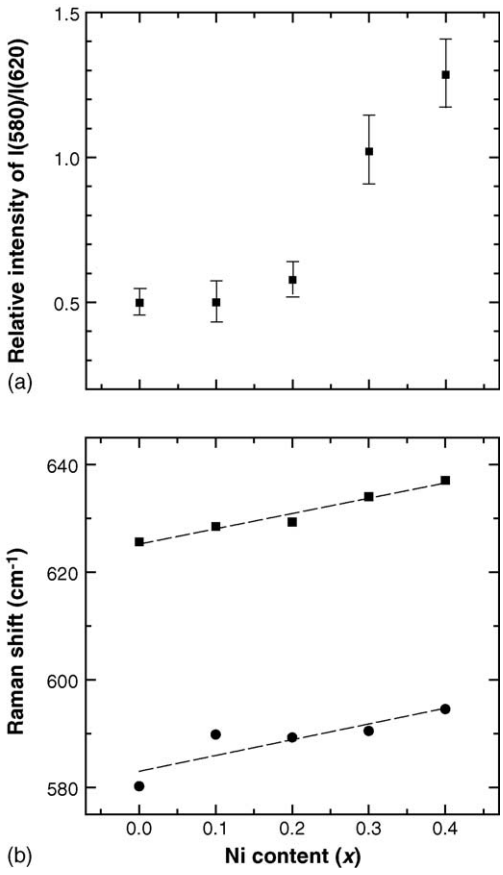

Fig. 3. (a) Plot of the relative intensity ratio of two main peaks at ~580 and ~620 cm^{-1}. (b) Variation of the frequency of two main peaks at ~580 (circles) and ~620 cm^{-1} (squares) upon Ni substitution. The dashed lines obtained from an interpolation are guides for eyes.

peaks show a distinct blue shift upon Ni substitution, indicating the reinforcement of Mn–O bonds caused by the oxidation of manganese ions (Fig. 3b). Over the present Ni-substitution region ($0 \le x \le 0.4$), the energies of these peaks are proportional to the Ni content. A pseudo-linear correlation between peak positions and Ni content (x) suggests that the substituted Ni ions have a similar chemical environment in the present substitution range of $0 \le x \le 0.4$. The other important change induced by the Ni substitution is the appearance of an intense peak at ~495 cm^{-1}. Previously this peak was interpreted as a $T_{2g}(2)$ phonon mode of the cubic spinel lattice [7]. However, judging from the fact that all of the Raman-active modes of $LiMn_2O_4$ are related not to the vibration of the transition metal but to those of oxygen and lithium [12], there is no reasonable origin for the prominent enhancement and the remarkable blue-shift of $T_{2g}(2)$ phonon line after the partial replacement of Mn with Ni. Hence this feature should not be ascribed to the lattice vibration of $T_{2g}(2)$ mode. On the other hand, NiO was reported to show an intense Ni–O vibration peak at around 500 cm^{-1} [18]. As illustrated in Fig. 4, there is a close structural similarity between rocksalt NiO and cubic spinel $LiMn_2O_4$, i.e. both structures are based on the cubic closest packed array of oxygen with transition metal ions occupying octahedral sites. In the light of this, it is highly feasible that the Ni–O vibration in cubic spinel lattice would have

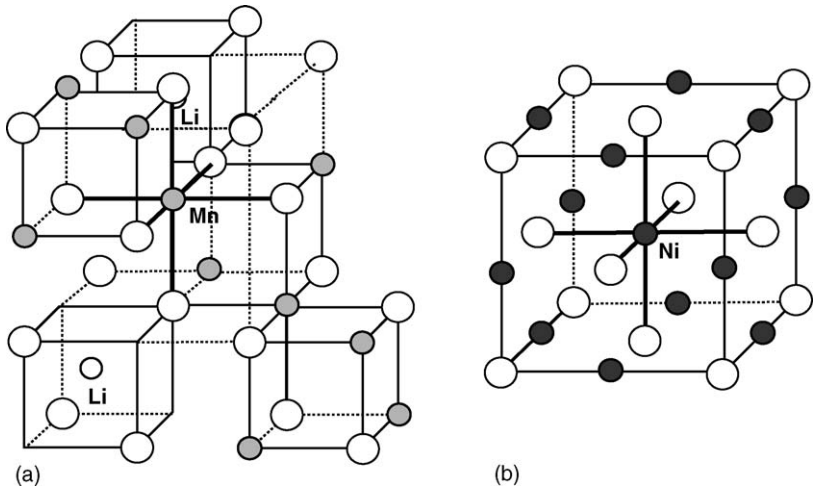

Fig. 4. Crystal structure around transition metal ions in (a) cubic spinel $LiMn_2O_4$ and (b) cubic rocksalt NiO. Small gray circles are manganese ions, small open circles are lithium ions, small black circles are nickel ions, and large open circles are oxygen ions.

a similar energy to that in rocksalt NiO. Based on this speculation, we can assign this peak as the Ni–O vibration of NiO_6 octahedra in spinel structure, rather than as the $T_{2g}(2)$ mode [11]. It is worthwhile to note here that the energy of this peak shows no remarkable change depending on the Ni content, suggesting similar bonding character of Ni ions in all of the present compounds.

3.3. Mn K-edge XAS analysis

The effect of Ni substitution on the chemical bonding nature of manganese ions has been investigated by using Mn K-edge X-ray absorption near-edge structure (XANES) analysis. Fig. 5 shows the Mn K-edge XANES spectra for $LiMn_{2-x}Ni_xO_4$ ($x = 0$, 0.2, and 0.4), in comparison with the reference spectra of the cubic spinel λ-MnO_2 and tetragonal spinel $Li_2Mn_2O_4$. The edge jump of the lithium nickel manganese oxides shifts toward the high-energy side with increasing Ni content, indicating the enhancement of the Mn oxidation state upon Ni substitution. This finding is in good agreement with the blue shift of the A_{1g} phonon lines corresponding to Mn–O vibrations (Fig. 3b). In the pre-edge region, all of the present samples exhibit weak features P and P′ corresponding to dipole-forbidden $1s \rightarrow 3d$ transitions. Even though they are not allowed by the electronic selection rule, $\Delta l = \pm 1$, the pre-edge peaks become discernible either due to quadrupole-allowed transitions and/or due to the mixing of 4p and 3d states [3]. In this context, the weak intensity of these features suggests that all the manganese ions in the samples under investigation are stabilized in octahedral sites with an inversion center. The position and shape of the pre-edge peaks are well-known to be closely related to the oxidation state of the absorbing ion and the local arrangement of backscattering ions [15]. As can be seen clearly from the inset of Fig. 5, the reference λ-MnO_2 with tetravalent manganese ions shows a stronger intensity of P′ than P, whereas only one feature P at lower energy appears for the $Li_2Mn_2O_4$ compound with trivalent manganese oxidation state. As the Ni content increases, the intensity of P′ becomes stronger, confirming the increase of the average Mn oxidation state. In the main-edge region, there are several features corresponding to the dipole-allowed transitions from the core 1s to the unoccupied 4p levels. Among them, the peak A has been assigned as a $1s \rightarrow 4p_\pi$ transition with a shakedown process [10,19]. Since the shakedown process is sensitive to the electrostatic repulsion between the $4p_\pi$ orbital and axial ligand, the intensity and the energy of the peak A provide a measure for probing the local structure around the manganese ion. In fact, a very strong peak A is observed at around 6547 eV for tetragonal spinel or monoclinic layered lithium manganese oxides [10], in which the trivalent manganese ion is commonly stabilized in the tetragonally distorted octahedra (Fig. 5). It is due to the fact that the elongation of ($Mn{-}O_{ax}$) bond facilitates the metal-to-ligand electron transfer along the c-axis and hence the shakedown process. The intensity of the peak A becomes

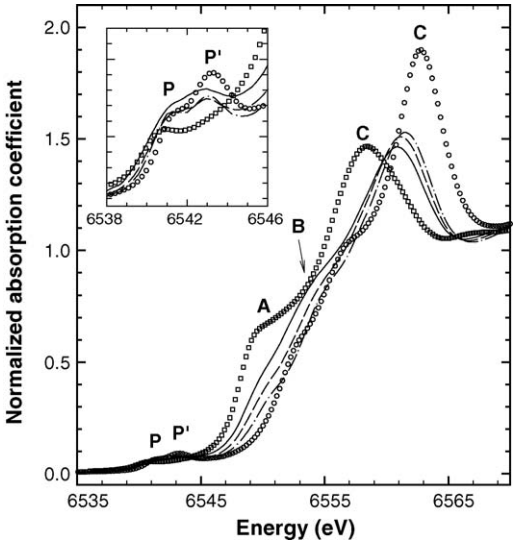

Fig. 5. Mn K-edge XANES spectra for cubic spinel $LiMn_{2-x}Ni_xO_4$ with $x = 0$ (solid lines), $x = 0.2$ (dashed lines), and $x = 0.4$ (dot–dashed lines), in comparison with those for the references $Li_2Mn_2O_4$ (squares) and λ-MnO_2 (circles). The inset presents an expanded view of pre-edge region for 6538–6546 eV.

smaller with increasing Ni content, underlining the shrinkage of the average ($Mn–O_{ax}$) bond distance and the depression of the tetragonal distortion. This is consistent with the increase of Mn oxidation state, giving rise to the decrease of Jahn-Teller active Mn^{III} concentration.

3.4. Ni K-edge XAS analysis

The influence of the Ni content on the oxidation state and local symmetry of nickel ions has been examined using Ni K-edge XANES/EXAFS spectroscopy. The Ni K-edge XANES spectra of $LiMn_{2-x}Ni_xO_4$ ($x = 0.2$ and 0.4) are plotted in Fig. 6, together with those of references NiO and $LiNiO_2$. The edge energies of lithium nickel manganese oxides are almost identical to that of $Ni^{II}O$ but lower than that of $LiNi^{III}O_2$, revealing the divalent oxidation state of nickel in these compounds. In the pre-edge region, a small peak P related to a dipole-forbidden transition from the core 1s to unoccupied 3d levels is observed for all the present compounds [3,10]. The weak intensity of the pre-edge peak P for $LiMn_{2-x}Ni_xO_4$ indicates that all of the substituted nickel ions are incorporated into the octahedral manganese site, not into the tetrahedral lithium site. In the main-edge region, there are several features corresponding to dipole-allowed $1s \rightarrow 4p$ transitions. The positions and shapes of main-edge peaks are nearly the same for both $LiMn_{1.8}Ni_{0.2}O_4$ and $LiMn_{1.6}Ni_{0.4}O_4$ compounds, underlining that the local chemical environment of substituted nickel ions shows no significant variation depending on the Ni content. To confirm this XANES result, the local geometric environment of nickel ions has been quantitatively determined by performing EXAFS analysis at Ni K-edge. The Fourier transforms (FTs) of k^3-weighted Ni K-edge EXAFS spectra for $LiMn_{2-x}Ni_xO_4$ and the reference NiO are plotted in Fig. 7a and the corresponding Fourier-filtered oscillations in Fig. 7b, respectively. For all of the present compounds, two FT

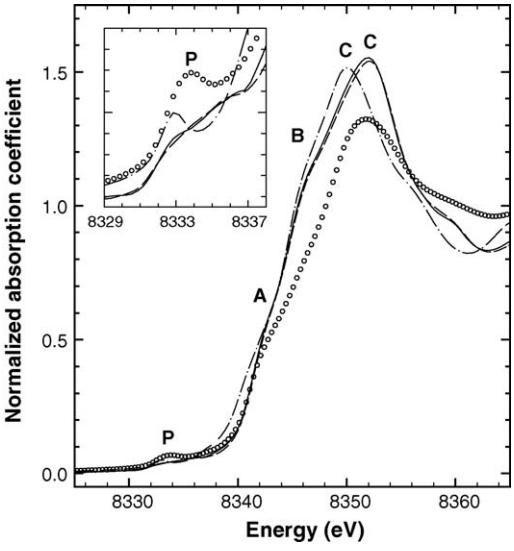

Fig. 6. Ni K-edge XANES spectra for $LiMn_{2-x}Ni_xO_4$ with $x = 0.2$ (solid lines) and $x = 0.4$ (dashed lines), in comparison with those for the references NiO (dot–dashed lines) and $LiNiO_2$ (circles). The inset presents an expanded view of pre-edge region for 8329–8338 eV.

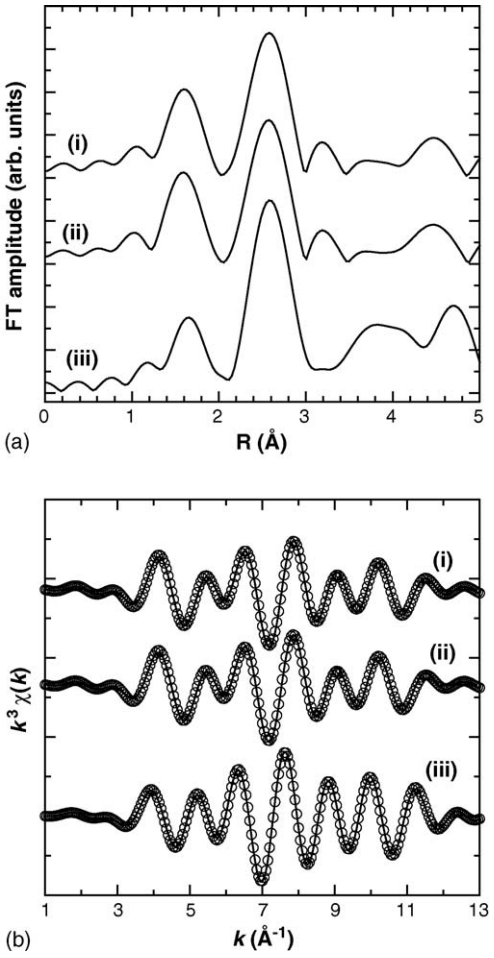

Fig. 7. (a) Fourier-transformed Ni K-edge EXAFS spectra and (b) their inverse Fourier transforms for (i) $LiMn_{1.8}Ni_{0.2}O_4$, (ii) $LiMn_{1.6}Ni_{0.4}O_4$, and (iii) NiO, respectively. In Fig. 7b, the solid lines and empty circles represent the fitted and experimental data, respectively.

peaks corresponding to the (Ni–O) and (Ni–M) shells (M = Mn or Ni) are observed at around 1.6 and 2.6 Å, which underscores that the substituted nickel ions are placed in regular octahedra. Such a local symmetry of nickel accounts for the absence of Jahn-Teller distortion in the divalent nickel ion with an electronic configuration of $[Ar]3d^8$. Regardless of the Ni content, both the lithium nickel manganates exhibit very similar spectra in the *R*- and *k*-spaces, strongly suggesting nearly the same local environment of nickel ion in these compounds. As shown in Fig. 7b, all of the present EXAFS data could be well reproduced on the basis of a regular NiO_6 octahedron with six neighboring metal ions at the same distance. As listed in Table 2, the nickel ions in both the $LiMn_{2-x}Ni_xO_4$ compounds are coordinated by six oxygen ligands at 2.04 Å. The estimated (Ni–O) distance is rather similar to the (Ni^{II}–O) distance in the reference NiO (2.07 Å), but much longer than the (Ni^{III}–O) distance in $LiNiO_2$ (1.93–1.94 Å) [17,20]. A slight difference in the (Ni–O) bond distance between $LiMn_{2-x}Ni_xO_4$ and NiO would be due to a smaller unit cell volume of the former than the latter. From the present EXAFS fitting results, it becomes clear that all the substituted nickel ions are stabilized in the octahedral sites of cubic spinel lattice without significant local structural change with

Table 2
Results of non-linear least square curve fittings for the Ni K-edge EXAFS spectra of cubic spinel $LiMn_{2-x}Ni_xO_4$ with $x = 0.2$ and 0.4, and the reference NiO

Sample	Bond	CN	ΔE (eV)	R (Å)	σ^2 ($10^{-3} \times$ Å)
$LiMn_{1.8}Ni_{0.2}O_4$[a]	Ni—O	6	4.37	2.04	6.59
	Ni—Mn, Ni	6	4.85	2.92	4.93
$LiMn_{1.6}Ni_{0.4}O_4$[a]	Ni—O	6	3.38	2.04	6.04
	Ni—Mn, Ni	6	4.14	2.92	4.73
NiO[b]	Ni—O	6	−0.44	2.07	6.49
	Ni—Ni	12	−1.67	2.94	6.92

[a] The curve-fit was performed for the range of $R = 1.043$–2.915 Å and $k = 3.70$–11.15 Å^{-1}.
[b] The curve-fit was performed for the range of $R = 1.166$–2.976 Å and $k = 3.50$–11.55 Å^{-1}.

the Ni content, which is in good agreement with the Ni K-edge XANES results. It is worthwhile to note here that the present XAS results are contrasted with the previous XPS results [7], in which the oxidation state of nickel decreases with the Ni content. Such an inconsistency between both results is due to the sensitivity of XPS to the surface species and that of XAS to the bulk ones [8]. In the light of this, the decrease of binding energy of Ni 2p XPS peak with the Ni content would be related to the presence of oxygen defect on the sample surface. It is highly feasible that more oxygen vacancies would be introduced for the heavily Ni-substituted compound than for the lightly Ni-substituted one, since the Ni ions have a lower oxidation state than the Mn ones. Taking into account the coordinatively unsaturated environment of the surface species, it is reasonable that the effect of oxygen vacancy is much more prominent on the surface species than on the bulk species, resulting in the distinct shift of XPS peak with the Ni content. In contrast, the present XAS results clarify that the chemical bonding nature of nickel ions in the bulk remains the same regardless of the Ni content. In this regard, the previously reported poor electrochemical performance of heavily Ni-substituted compounds in the 3 V region cannot be explained from the viewpoint of the dependence of Ni bonding character on the substitution rate [6,7]. Instead, the variation of electrochemical property with the Ni content seems to be related to the stability of the NiO_6 octahedra. Previously we have reported that the substituted NiO_6 octahedra in the cubic spinel lattice experience severe structural changes upon Li intercalation [3]. Thus, the high concentration of unstable NiO_6 octahedra in the heavily Ni-substituted compound should give rise to the depression of the overall structural stability and electrochemical cyclability in the 3 V region. In the case of the lightly substituted compound, the stabilization of spinel lattice through the reinforcement of Mn—O bonds upon the Ni-substitution prevails over the negative effect of unstable NiO_6 octahedra, leading to the improvement of electrochemical performance. It is worthwhile to mention that, in contrast to the present substituted compound with $0 < x < 0.4$, a spinel compound $LiMn_{2-x}Ni_xO_4$ with a higher Ni content ($x > 0.5$) should have the mixed oxidation states of Ni^{II}/Ni^{III} or oxygen defects to meet an electroneutrality principle. For such a higher Ni substitution region, the change of local environment of nickel ions would affect distinctly the electrochemical properties and stability of Ni-substituted spinel compound especially in a high potential region of ~4.7 V.

4. Conclusions

In this study, we have clearly demonstrated from micro-Raman and XAS analyses that divalent nickel ions exist in the octahedral sites of cubic spinel lattice of lithium manganate and the chemical bonding nature of the substituted nickel ions does not show any significant changes depending on the substitution rate. Thus, as the Ni content increases, the average oxidation state of the manganese ions becomes monotonously enhanced along with the resultant reinforcement of the Mn—O bonds. On the basis of the experimental findings presented here, we suggest that the previous XPS results showing the dependence of the Ni valence state on the substitution rate would originate from the surface-sensitivity of XPS, not from a change of the Ni bonding character in the bulk state. In the light of this, we can attribute the poor electrochemical performance of heavily Ni-substituted compounds in the 3 V region to low structural stability of the NiO_6 octahedra upon Li intercalation, rather than to a variation of the Ni bonding character depending upon the Ni content.

Acknowledgments

This work was performed by the financial support of National R&D programs' of the Ministry of Science and Technology (MOST), Republic of Korea, and supported partly by the SRC/ERC program of MOST/KOSEF (grant: R11-2005-008-00000-0). The experiments at PLS were supported in part by MOST and POSTECH.

References

[1] (a) M.M. Thackeray, Prog. Solid State Chem. 25 (1997) 1;
(b) J.H. Choy, D.H. Kim, C.W. Kwon, S.J. Hwang, Y.I. Kim, J. Power Sources 77 (1999) 1.
[2] R.J. Gummow, A. de Kock, M.M. Thackeray, Solid State Ionics 69 (1994) 59.
[3] S.J. Hwang, H.S. Park, J.H. Choy, G. Campet, J. Phys. Chem. B 105 (2001) 335.
[4] (a) Y.K. Sun, Y.S. Jeon, H.J. Lee, Electrochem. Solid State Lett. 3 (2000) 361;
(b) M.R. Palacin, F. Le Cras, L. Seguin, M. Anne, Y. Chabre, J.M. Tarascon, G. Amatucci, G. Vaughan, P. Strobel, J. Solid State Chem. 144 (1999) 361.
[5] (a) M. Hosoya, H. Ikuta, M. Wakihara, Solid State Ionics 111 (1998) 153;
(b) G. Pistoia, A. Antonini, R. Rosati, C. Bellitto, G.M. Ingo, Chem. Mater. 9 (1997) 1443.

[6] (a) I. Taniguchi, D. Song, M. Wakihara, J. Power Sources 109 (2002) 333;
(b) Y.K. Sun, D.W. Kim, Y.M. Choi, J. Power Sources 79 (1999) 231;
(c) P. Strobel, A.I. Palos, M. Anne, F. Le Cras, J. Mater. Chem. 10 (2000) 429.
[7] Y.J. Wei, L.Y. Yan, C.Z. Wang, X.G. Xu, F. Wu, G. Chen, J. Phys. Chem. B 108 (2004) 18547.
[8] N. Treuil, C. Labrugère, M. Menetrier, J. Portier, G. Campet, A. Deshayes, J.C. Frison, S.J. Hwang, S.W. Song, J.H. Choy, J. Phys. Chem. B 103 (1999) 2100.
[9] S.J. Hwang, D.H. Park, J.H. Choy, G. Campet, J. Phys. Chem. B 108 (2004) 12713.
[10] (a) S.J. Hwang, H.S. Park, J.H. Choy, G. Campet, J. Phys. Chem. B 104 (2000) 7612;
(b) H.S. Park, S.J. Hwang, J.H. Choy, J. Phys. Chem. B 105 (2001) 4860.
[11] K. Dokko, M. Mohamedi, N. Anzue, T. Itoh, I. Uchida, J. Mater. Chem. 12 (2002) 3688.
[12] (a) B. Ammundsen, G.R. Burns, M.S. Islam, H. Kanoh, J. Rozière, J. Phys. Chem. B 103 (1999) 5175;
(b) H. Kanoh, W. Tang, K. Ooi, Electrochem. Solid State Lett. 1 (1998) 17.
[13] W. Huang, R. Trech, J. Power Sources 81–82 (1999) 616.
[14] S.J. Hwang, H.S. Park, J.H. Choy, Solid State Ionics 151 (2002) 275.
[15] S.J. Hwang, C.W. Kwon, J. Portier, G. Campet, H.S. Park, J.H. Choy, P.V. Huong, M. Yoshimura, M. Kakihana, J. Phys. Chem. B 106 (2002) 4053.
[16] J.H. Choy, S.J. Hwang, N.G. Park, J. Am. Chem. Soc. 119 (1997) 1624.
[17] R.D. Shannon, Acta Crystallogr. A 32 (1976) 751.
[18] (a) S.H. Lee, H.M. Cheong, N.G. Park, C.E. Tracy, A. Mascarenhas, D.K. Benson, S.K. Deb, Solid State Ionics 140 (2001) 135;
(b) P. Delichere, S. Joiret, A. Hugot-le Goff, K. Bange, B. Hetz, J. Electrochem. Soc. 135 (1998) 1856.
[19] C.R. Horne, U. Bergmann, M.M. Grush, R.C.C. Perera, D.L. Ederer, T.A. Callcott, E.J. Cairns, S.P. Cramer, J. Phys. Chem. B 104 (2000) 9587.
[20] I. Nakai, K. Takahashi, Y. Shiraishi, T. Nakagome, F. Nishihawa, J. Solid State Chem. 140 (1998) 145.